Antarct. Meteorite Res., **12**, 36–56, 1999

EFFECTS OF TERRESTRIAL WEATHERING ON THE MATRIX MINERALOGY OF COLONY CO3 CHONDRITE

Takaaki NOGUCHI[1], Kei-ichi ISHIKAWA[1]* and Kiyotaka NINAGAWA[2]

[1] *Department of Materials and Biological Sciences, Ibaraki University, Bunkyo 2-chome, Mito 310-8512*

[2] *Department of Applied Physics, Faculty of Science, Okayama University of Science, Ridai-cho 1-1, Okayama 700-0005*

Abstract: Colony is the least metamorphosed CO chondrite (CO3.0). However, it is badly weathered. In order to show both primary and secondary features of the matrix and discuss the effects of terrestrial weathering on the matrix mineralogy of Colony, we performed combined SEM, EPMA, CL, and TEM studies on this meteorite. EPMA data of the matrix of Colony show that matrix composition was changed by terrestrial weathering. The matrix composition can be represented by three hypothetical components: an Fe-rich component (Fe hydroxide-rich weathering products), a component with olivine-like composition, and an Fe-poor, Si-rich component. TEM observation reveals that the matrix contains abundant Fe-rich poorly crystalline interstitial materials, abundant ferroan olivine (Fa_{50}-Fa_{60}), less abundant magnesian low-Ca pyroxene (En_{99-90}), magnetite, and minor amounts of spinel group minerals, troilite, and rare Ca-rich pyroxene. Among these phases, anhydrous minerals are primary minerals. The Fe-rich component estimated from EPMA data is composed of abundant Fe-enriched, nearly amorphous material, minute phyllosilicates (mainly saponite, serpentine, and minor amounts of chlorite and montomorillonite), and goethite. The Fe-poor, Si-rich component estimated from EPMA data is also composed of basically the same but seems to contain more phyllosilicates than the Fe-rich one. Matrix olivine crystals often contain planar defects parallel to (001). Such planar defects were probably formed in the initial stage of iddingsite formation by terrestrial weathering.

1. Introduction

Petrologic studies of CO chondrites show that CO chondrites experienced metamorphism (*e.g.*, SCOTT and JONES, 1990; SEARS *et al.*, 1991). Among CO chondrites, type 3.0–3.1 CO chondrites have some features that are rare in the higher types. Mesostases in type I chondrites and very fine-grained matrix produce yellow and red CL, respectively (SEARS *et al.*, 1991). SCOTT and JONES (1990) classified Colony and ALHA 77307 as the least metamorphosed CO chondrites (CO3.0), and SEARS *et al.* (1991) showed that these meteorites and LEW85332 (CO3.0) are compositionally anomalous. RUBIN *et al.* (1985) described that Colony is badly weathered. We investigate the matrix of the Colony meteorite which is one of the least metamorphosed CO chondrites, using scanning electron microscope (SEM), electron microprobe analyzer (EPMA),

* Present address: Mito City Hall, Chuo 1-4-1, Mito 310-8610.

cathodeluminescence (CL), and transmission electron microscope (TEM). We will show both primary and secondary features of the matrix and discuss the effects of terrestrial weathering on the matrix mineralogy of Colony.

2. Materials and Experimental Methods

The samples for TEM observation were prepared from demountable polished thin sections (PTS'). A detailed SEM observation was carried out with a JEOL JSM-840 equipped with an energy dispersive spectrometer (Link system). EPMA analysis (focused beam) was performed by a JEOL JXA-733 microprobe operated at 15 kV accelerating voltage and 9 nA beam current for silicates and oxides. After petrographic studies by SEM and EPMA, the areas of interest for TEM study were drilled by a precision cutting device and then hand picked from the PTS'. The samples were then prepared for TEM studies by conventional ion-milling techniques, using a GATAN ion-milling machine. Low to high-resolution images, selected area electron diffraction patterns, and microanalysis were obtained using JEOL JEM-2000 FXII TEM operating at 200 kV. A Philips DX4 energy dispersive X-ray analysis system was used to obtain quantitative analytical data employing the Cliff-Lorimer thin film approximation for data reduction. Experimental k factors were determined from many mineral standards. Effects of sample thickness on k factors were considered by regarding k factors as functions of peak intensities.

Correction by the BENCE and ALBEE (1968) method was used for the analyses of silicates and oxides. Special deconvolution programs were applied to correct for X-ray overlaps of K_β and K_α lines between some elements such as Ti and V and Ca and P. Detection limits of EPMA analysis based on the Bence and Albee correction for minor elements (wt%) were reported in NOGUCHI (1995).

For CL observation of the samples, we used a Premier American Technologies 'ELM-3 Luminoscope systems' attached to an optical microscope with an electron beam of 15 keV and 0.5 mA, 35 mm Camera and Fuji Super G Ace 800 film, and exposures of 10–60 min.

3. Results

3.1. SEM observation

SEM observation shows that the matrix of Colony is composed mainly of very fine-grained (mainly sub-μm) materials. Some olivine crystals which are $>3\,\mu$m across are also observed along with the fine-grained materials. Thin veins $<5\,\mu$m thick (bright veins in back-scattered electron images (BEIs)) are often observed (Fig. 1). Their occurrences and chemical compositions indicate that they are thin "limonite" veins. Figure 2 shows that there are areas which have different brightness in BEIs within the matrix. Darker areas are separated by sinuous brighter areas. The fine-grained matrix tends to become darker with distance from thick veins (about $>5\,\mu$m across) (Fig. 1b). Matrix around altered Fe-Ni metal grains (isolated grains in matrix and spherules on the surfaces of chondrules) are often bright in BEIs. Fine-grained matrix near finer veins is not always bright (Fig. 1a). Figure 1b shows that there are two thick

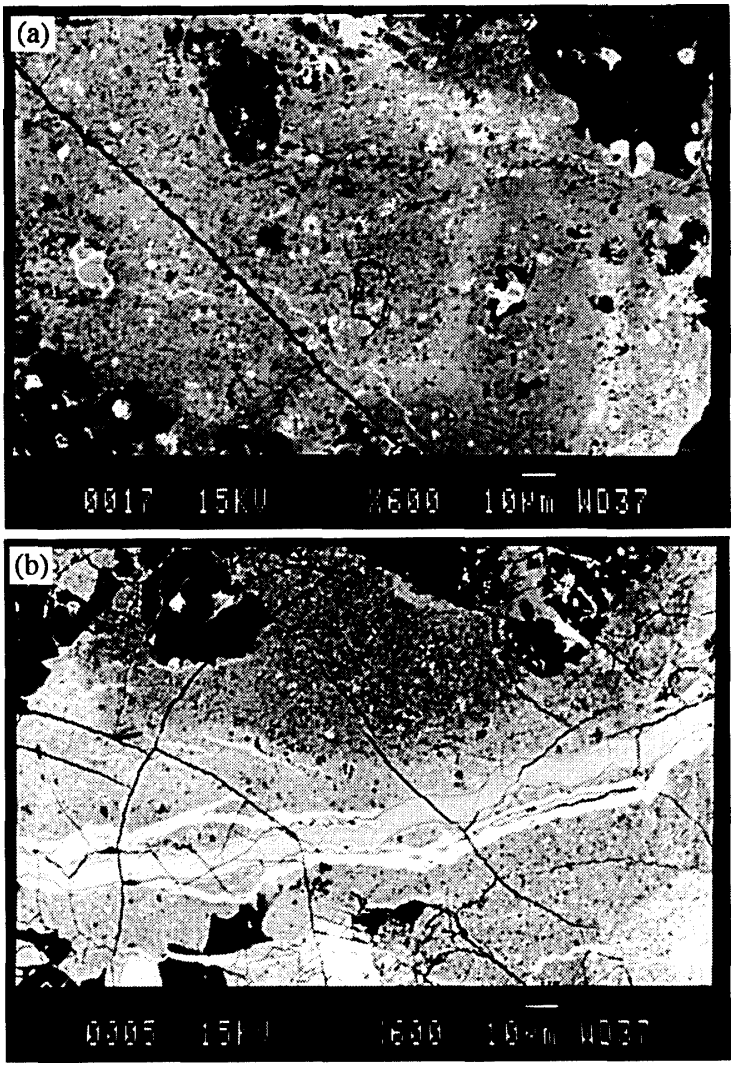

Fig. 1. A backscattered electron image (BEI) of fine-grained matrix of Colony. The majority of fine-grained matrix is composed of sub-μm sized materials with fragments of olivine and pyroxene and chondrules. Large unaltered Fe-Ni metal grains are absent in the matrix. (a) In the fine-grained matrix, relatively darker areas are surrounded by brighter areas. Bright areas are usually related to altered Fe-Ni metal grains on the surfaces of chondrules and in matrix. (b) A BEI of fine-grained matrix near a composite "limonite" vein. Brightness of fine-grained matrix in the BEI tends to be darker when one goes away from the vein. The vein is composed of a bright "limonite" vein, which was cut later by a gray "limonite" vein.

"limonite" veins which were formed at different times. "Limonite" is not a mineral name but a kind of "field-name". In this paper, the term is used for a weathering product with high FeO content, and low but various SiO_2 content. A thinner and brighter vein is cut by a thicker and darker vein. These photomicrographs show that "limonite" veins and aggregates were not formed at the same time.

3.2. Chemical composition of matrix

Brightness in BEIs depends on the average atomic number of each material (*e.g.* LLOYD, 1987). Figure 2 shows the relationships between oxide wt% of major elements and the distance from the thick bright vein in Fig. 1b. Obviously, total FeO (FeO plus Fe_2O_3) wt% increases, and oxide wt% of SiO_2, MgO, Al_2O_3, and total wt% decrease, as the distance from the vein decreases ($<10\mu$m). These data suggest that the average atomic number of matrix increase near the vein. It is consistent with the brightness of BEI of the matrix in Fig. 1b.

The brightness of the matrix in BEIs is difficult to treat quantitatively. FeO wt% of the matrix, however, seems to correlate well with the brightness in BEIs. Therefore,

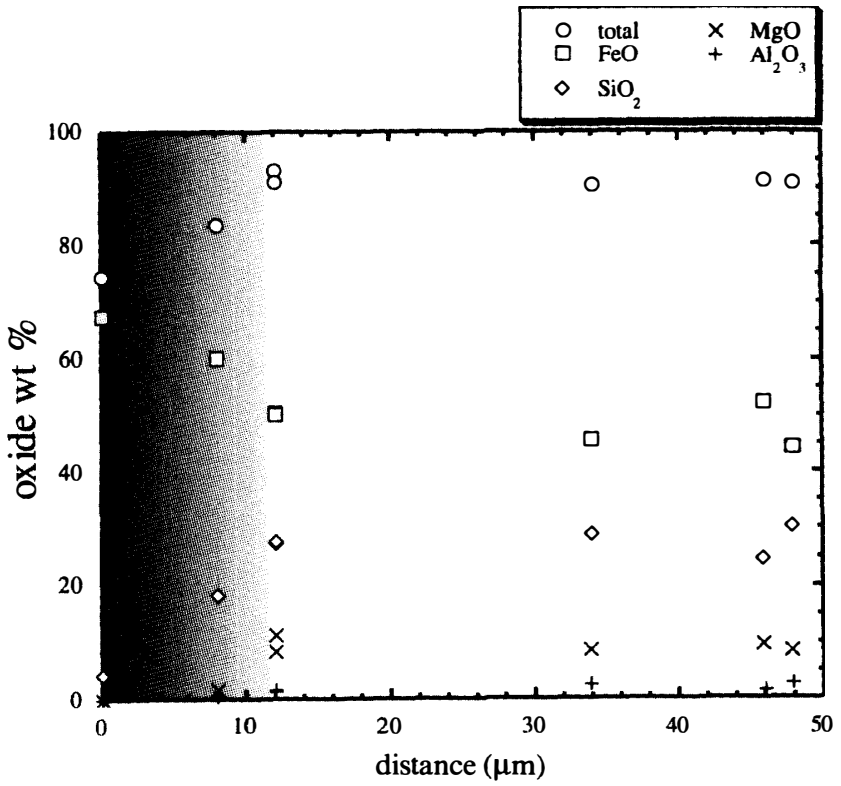

Fig. 2. The relation between distance from a "limonite" vein vs some oxide wt% of fine-grained matrix. A shaded area indicates where remarkable compositional changes were observed. These data were measured by electron microprobe (EPMA).

FeO wt% was used instead of the brightness in BEI photomicrographs. In Figs. 3 and 4, the matrix of Colony was divided into four types on the basis of FeO wt% (matrix 1: <40; matrix 2: 40 to 50; matrix 3: 50 to 60; matrix 4: >60), in order to see the relations between compositional features and the brightness of the matrix in BEIs. The boundaries between each type are arbitrary.

Figure 3 displays some interelemental correlations of the matrix of Colony. There is a negative correlation between FeO and SiO_2 concentrations (Fig. 3a). This negative correlation suggests that the matrix is basically represented as a two-component mixture: SiO_2-rich and FeO-rich components. Total wt% of the matrix is nearly constant except for matrix near "limonite" veins and aggregates, as shown in Fig. 2, because SiO_2 and FeO are the main constituent oxides. Average chemical compositions of the fine-grained matrix of Colony support this tendency (Table 1).

Figures 3b and 3c show that there are positive correlations among Al_2O_3 and CaO, and among Al_2O_3 and Na_2O+K_2O wt%. These elements may be kept in the same carrier. Al_2O_3, CaO, Na_2O+K_2O (Na_2O occurs in trace amounts) contents tend to decrease as FeO content increases. As in Fig. 4a, from these diagrams, the matrix is interpreted as a mixture of an Al_2O_3-, CaO-, $[Na_2O+K_2O]$-rich component and a component which is poor in these oxides. Table 1 shows that average Al_2O_3, CaO, and K_2O decrease as average FeO increases. Average SO_3 increases as average FeO

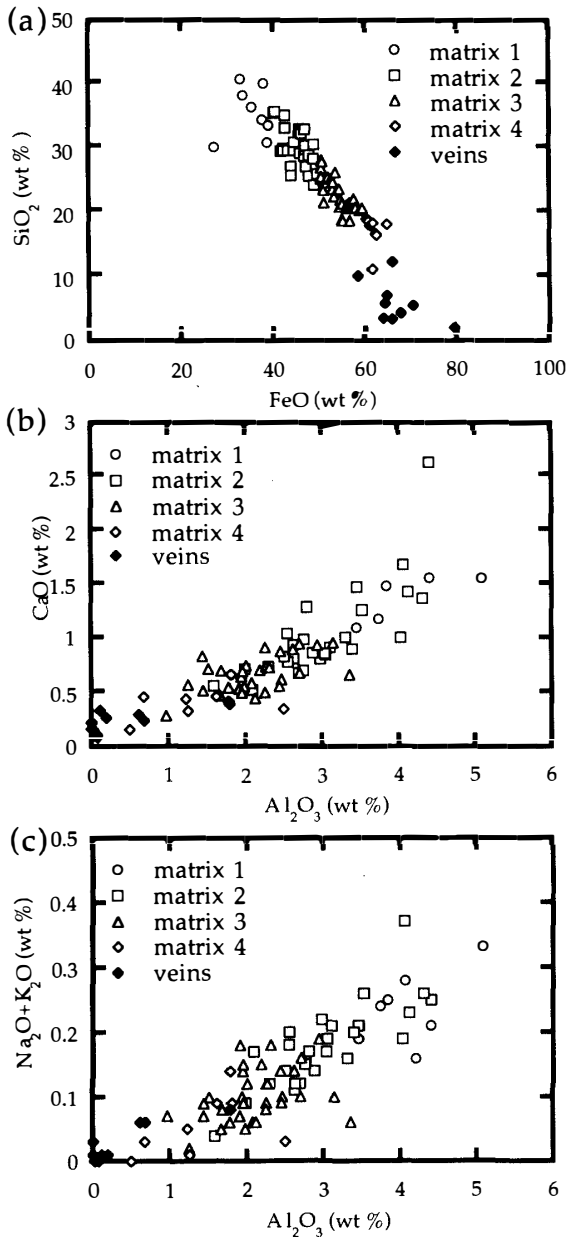

Fig. 3. The relations among some oxide wt% in fine-grained matrix. EPMA data. Matrices 1 to 4 were divided by FeO wt%: matrix 1 (open circle): <40; matrix 2 (open square): 40 to 50; matrix 3 (open triangle): 50 to 60; matrix 4 (open diamond): >60, respectively. These names are common to Fig. 5 and Table 1. Veins in the legend (filled diamond) means "limonite"-rich veins and aggregates.

increases. Average Cr_2O_3 and NiO values also decrease as average FeO increases, but these values in the veins are higher than the values of the entire matrix. Average P_2O_5 content shows a similar relationship to average FeO as shown in Cr_2O_3 and NiO. Table 1 also lists the average chemical compositions of an opaque matrix of Colony by RUBIN *et al.* (1985). Their data are similar to the average data of matrix 2 in Table 1. However, average FeO content of matrix 2 is much higher than that of RUBIN *et al.* (1985). This compositional difference is probably due to the difference of the analytical method. Because our data were obtained using a focused beam technique, we avoided small olivine and pyroxene fragments, and chondrule fragments which are usually magnesian. On the other hand, in RUBIN *et al.* (1985), a broad-beam technique was used and therefore such olivine and pyroxene fragments were included when they were

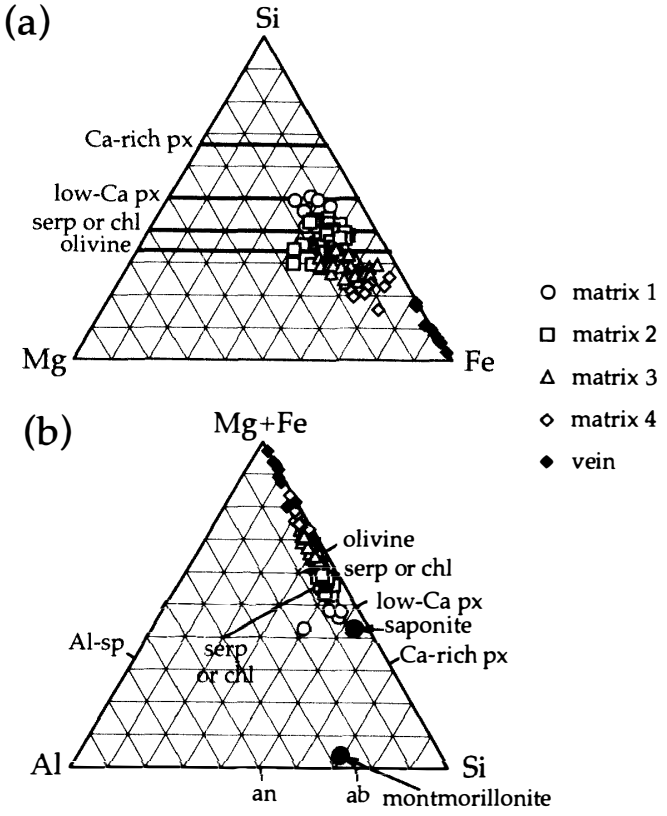

Fig. 4. Major element compositions of the fine-grained matrix and "limonite" veins and aggregates are plotted on ternary Si-Mg-Fe and [Mg+Fe]-Al-Si diagrams. Abbreviations are the same in Fig. 3.

analyzed.

Compositions of "limonite" veins and aggregates suggest that they are mainly composed of hydrous iron oxides with some amounts of SiO_2 (6.8 SiO_2 wt% on average). It is not clear whether SiO_2 is incorporated in hydrous iron oxides or whether it exists as an amorphous SiO_2-rich material.

Major element compositions of the fine-grained matrix and the weathering veins are plotted on ternary Si-Mg-Fe and [Mg+Fe]-Al-Si diagrams (Fig. 4). In Fig. 4a, the matrix poorer in FeO content (correspond to darker in BEIs) has higher Si/(Si+Mg+Fe) ratios than the matrix richer in FeO (correspond to brighter regions in BEIs). This diagram shows that "limonite" veins and aggregates contain almost no Mg. On the other hand, even the matrix rich in FeO contains a considerable amount of Mg. This diagram also suggests that the matrix of Colony can be represented as a mixture of three major components, which can not be distinguished from the two-component diagrams in Fig. 3. They are an Fe-poor and Si-rich component, a component with olivine-like atomic ratios, and an Fe-rich component.

All the three major components are poor in Al (Fig. 4b). This diagram suggests that the Fe-poor and Si-rich component in Fig. 4a contains a considerable amount of saponite or poorly crystalline materials with saponite-like compositions. Al_2O_3, CaO, and K_2O are probably included in the Fe-poor, Si-rich component.

3.3. CL of matrix

Figure 5 is a cathodeluminescence photomicrograph of Colony. Because the exposure time for this photomicrograph is very long (60 min), the color valance may be

Table 1. Average microprobe analyses of fine-grained matrix in Colony.

	fine-grained matrix 1		fine-grained matrix 2		fine-grained matrix 3		fine-grained matrix 4		veins		opaque matrix	
	average	1 σ	average	1 σ	average	1 σ	average	1 σ	average	1 σ	average	1 σ
No.	8		27		33		8		9		25	
SiO_2	35.3	4.0	29.7	3.0	22.4	2.8	16.6	2.4	6.0	3.4	25.6	2.4
TiO_2	0.23	0.50	<0.08		<0.08		<0.08		<0.08		0.11	0.05
Al_2O_3	5.0	2.5	3.0	0.7	2.1	0.5	1.4	0.7	0.39	0.59	2.5	0.8
Cr_2O_3	0.38	0.16	0.38	0.10	0.31	0.07	0.21	0.09	0.63	0.78	0.38	0.08
FeO	35.2	4.0	45.2	2.7	54.1	2.8	61.7	1.4	66.7	5.7	46.0	5.1
NiO	2.5	0.6	2.0	0.5	1.8	0.5	1.7	0.6	2.7	1.7	2.0	0.4
MnO	<0.10		<0.10		<0.10		<0.10		<0.10		0.32	0.08
MgO	7.1	1.9	7.8	3.0	7.2	2.4	5.6	2.5	0.14	0.18	11.6	2.7
CaO	2.8	2.9	1.0	0.4	0.66	0.16	0.40	0.14	0.23	0.09	0.79	0.79
Na_2O	<0.06		<0.06		<0.06		<0.06		<0.06		0.13	0.13
K_2O	0.18	0.05	0.14	0.06	0.07	0.03	<0.05		<0.05		0.14	0.07
P_2O_5	0.35	0.08	0.38	0.17	0.25	0.15	0.10	0.12	0.44	0.60	0.41	0.12
SO_3	0.18	0.13	0.21	0.07	0.33	0.09	0.49	0.16	0.57	0.31	0.87	0.72
total wt %	89.2		89.9		89.3		88.3		77.8		90.9	

No.: number of analyses

b. d.: below detection limits

fine-grained matrix 1: fine-grained matrix with < 40 FeO wt %

fine-grained matrix 2: fine-grained matrix with 40-50 FeO wt %

fine-grained matrix 3: fine-grained matrix with 50-60 FeO wt %

fine-grained matrix 4: fine-grained matrix with > 60 FeO wt %

average composition of opaque matrix: data from RUBIN *et al.* (1985)

total Fe oxide wt % is displayed as FeO wt %

changed due to deviation from the reciprocity law of film. However, it is clear that the matrix is not luminescent even in this photomicrograph. In this figure, mesostases in some chondrules show blue and yellow CL, and overexposed areas are white. Because Fe-rich materials do not show CL, our data are consistent with microprobe data of the matrix which show higher Fe/(Fe+Mg) ratio than those of other CO3s (RUBIN *et al.*, 1985).

3.4. TEM observation and analysis

TEM observation showed that the fine-grained matrix of Colony is composed mainly of sub-μm sized grains of abundant olivine, and less abundant low-Ca pyroxene and magnetite with abundant Fe-rich, poorly crystalline material which fills the interstices of these unhydrous minerals (Fig. 6). Minor matrix minerals are spinel group minerals (both chromian and aluminous), troilite, and rare Ca-rich pyroxene.

Olivine

Olivine in Colony is Fe-rich and fine-grained ($<0.3\,\mu$m in diameter, in most cases). Shapes of olivine are rounded, irregular, and sometimes subhedral. Many olivine

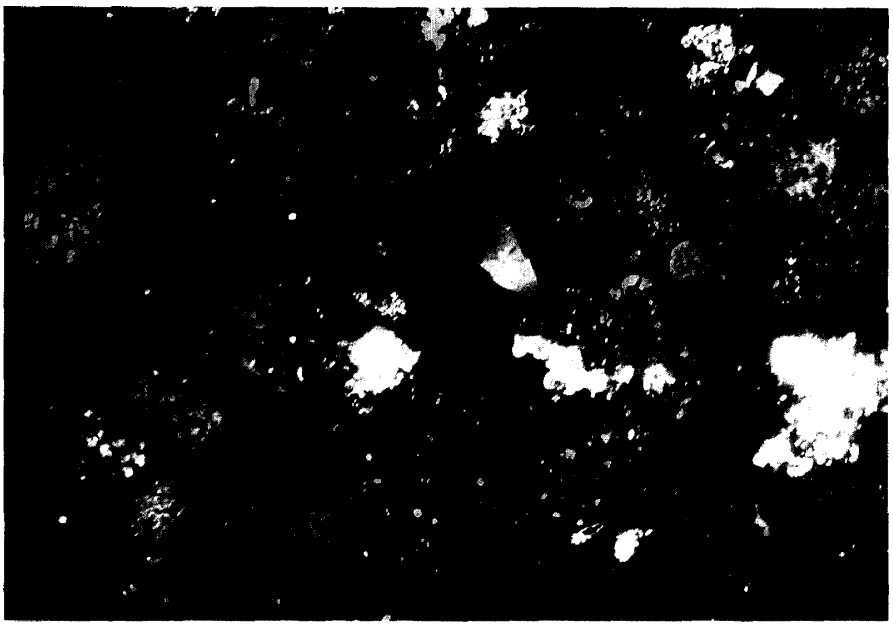

Fig. 5. A cathodeluminescence photomicrograph of Colony. Matrix is not luminescent in spite of long exposure time (60 min). On the other hand, Magnesian olivine and pyroxene and chondrule glasses show red, blue, and yellow luminescence. Over exposed areas appear to be white. The width of this photograph is 1.27 mm.

grains are altered to Fe-rich, poorly crystalline materials (Table 2, Fig. 6b). This figure suggests that primary grain sizes of many matrix olivine grains were fairly larger than present sizes. Relict olivine grains contain semi-periodic channels that are normal or nearly normal to (001) of olivine (Figs. 6b and 7). Because these defects always appear to be channels when viewed from the directions normal to c* of olivine, their three-dimensional shapes are planar rather than linear, parallel or sub-parallel to (001) of olivine. These defects occur in semi-periodic fashion (Fig. 7). Their intervals are about 15 nm. Due to close existence of the defects, diffraction spots display streaks parallel to the c* direction of olivine on a selected area electron diffraction (SAED) pattern (Fig. 7a). Crystal structure of olivine is disturbed and replaced by materials with low crystallinity within these planar defects (Fig. 7b). Incipience of formation of these defects appears as pits on the surface of olivine (Fig. 7b). Other defects such as dislocations are rare in the matrix olivine.

Fa mol% is different between unaltered matrix olivine (without planar defects) and altered matrix olivine (including planar defects). Most of the unaltered olivine is concentrated between Fa_{50} to Fa_{60}. On the other hand, altered olivine is more Fe-rich (Fig. 8a). There is, however, an ambiguity whether this difference is apparent or not, because materials which fill the planar defects are probably much more Fe-rich than the host olivine. Both unaltered and altered matrix olivines contain 0.2–0.8 wt% MnO (Fig. 8b and Table 2). Iron and manganese ratios in these olivines are near the ratio with solar abundance (Fig. 8b). Fa mol% and FeO *vs* MnO ratios of the matrix olivine are quite different from those of olivine in chondrules (Figs. 8c and 8d).

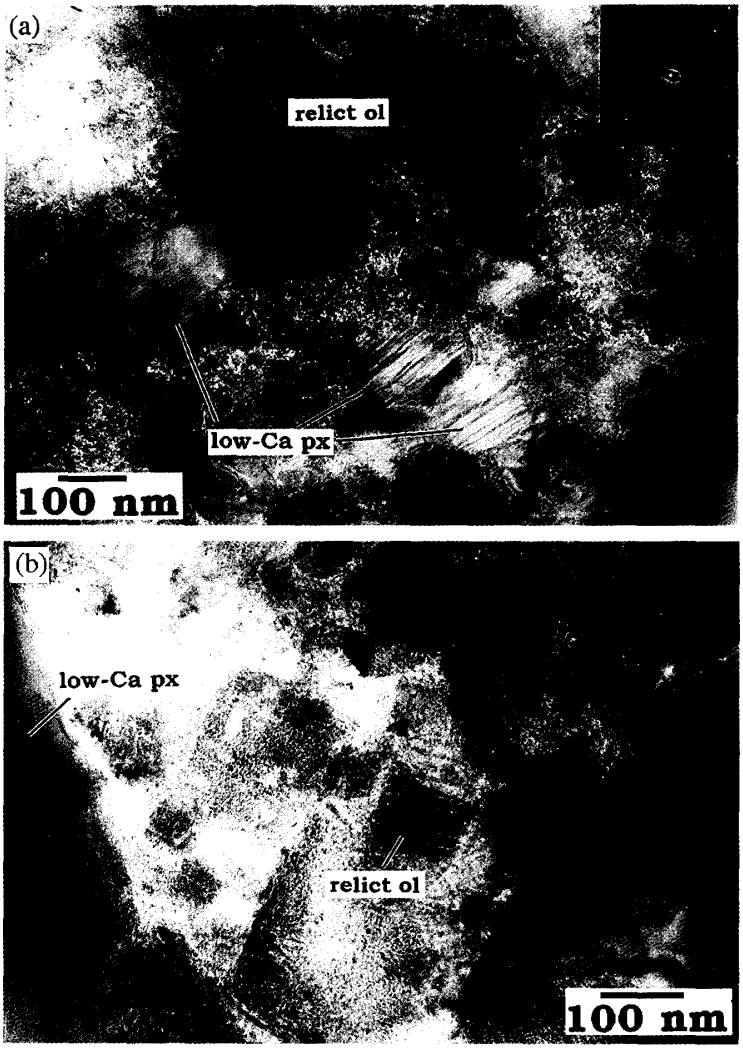

Fig. 6. Low-magnification bright-field TEM images of fine-grained matrix of Colony. (a) Fine-grained matrix is composed mainly of olivine, low-Ca pyroxene, and interstitial materials. The selected area electron diffraction (SAED) pattern shows that the interstitial materials are almost amorphous. Some diffraction spots in the SAED pattern are due to olivine and pyroxene in the matrix. (b) Matrix olivine is replaced by the poorly crystalline interstitial materials. The relicts of matrix olivine have defects with a channel-like appearance. Low-Ca pyroxene seems not to have been altered. Fibrous materials can be found in the upper-right part of this photograph.

Pyroxene

Low-Ca pyroxene crystals in the matrix are less abundant than olivine, and have similar sizes to olivine. They are rounded to irregularly elongated (Figs. 6a and 9). Most of them are low-Ca clinopyroxene with stacking disorder on (100) due to minor intergrowth of orthopyroxene (Fig. 9). The majority of low-Ca pyroxene does not show clear evidence for alteration, although euhedral low-Ca pyroxene is very rare.

The majority of matrix low-Ca pyroxene are very magnesian (<4 Fs mol%) like those in chondrules (Table 2, Figs. 10a and 10c). However, MnO contents are different between those in matrix and those in chondrules. The majority of low-Ca pyroxene in matrix contains about 0.6–0.9 wt% MnO (Fig. 10b). On the other hand, most of the low-Ca pyroxene in chondrules contains $<$ about 0.2 wt% MnO (Fig. 10d). Matrix low-Ca contains 1–2 wt% of Al_2O_3, Cr_2O_3, and CaO (Table 2).

Ca-rich pyroxene is very rare. Only one crystal was observed.

Magnetite

Magnetite grains which are large enough to be identified by combined SEM

Table 2. Selected AEM analyses of some components of Colony matrix.

mineral (or mixture of minerals)	olivine	low-Ca pyroxene	magnetite	interstitial material	interstitial material	interstitial material
SiO_2	33.3	57.0	n. a.	12.0	15.5	44.7
Al_2O_3	n. a.	2.4	n. a.	2.1	3.0	8.1
Cr_2O_3	n. a.	1.3	0.8	n. a.	n. a.	n. a.
FeO	48.0	2.0	99.2	72.0	70.1	30.5
NiO	n. a.	n. a.	n. a.	1.9	1.4	4.9
MnO	0.4	0.8	n. a.	0.2	0.4	n. a.
MgO	18.4	34.0	n. a.	1.7	3.3	4.6
CaO	n. a.	2.4	n. a.	1.8	1.4	2.7
Na_2O	n. a.	n. a.	n. a.	3.5	n. a.	n. a.
K_2O	n. a.	n. a.	n. a.	1.2	1.5	4.4
SO_3	n. a.	n. a.	n. a.	3.6	3.4	n. a.
total wt %	100.0	100.0	100.0	100.0	100.0	100.0

All data are 100 % normalized.

n. a.: not analyzed. (Peaks were not detected in EDS spectra.)

Anhydrous minerals were measured by 30 to 100 nm electron beams and intersitital materials were measured by 150 to 300 nm electron beams.

observation and electron microprobe analysis were not found in the matrix of Colony. However TEM observation revealed that there are sub-μm sized ($<0.5\mu$m in diameter, in most cases) isolated, subhedral magnetite grains in the matrix (Fig. 11a). Crystallinity of these magnetite grains is well developed. These magnetite grains show no evidence of alteration. Magnetite grains contain a small amount of Cr (<1 wt% Cr_2O_3), but does not contain Al, Ti, and Mn (Table 2).

Spinel group minerals

Spinel group minerals except for magnetite are also found in the matrix. Both chromian and aluminous spinels were observed. Their grain sizes and shapes are similar to those of magnetite.

Troilite

In the matrix of Colony, there are relatively large troilite grains (1–2μm across), however, sub-μm sized troilite grains are rare. The majority of such large troilite grains show comb-like alteration texture which is similar to the case of olivine. Parallel to subparallel channels normal to (001) of troilite are observed near the surfaces of troilite grains. The channels are spaced about 40–50 nm apart. Like the case of olivine, the defects appear as channels when they are viewed from direction normal to (001) of the host troilite (Fig. 11b). Therefore, these defects are planar in three dimensions. Materials with low crystallinity are filled within the defects. The thickness of the defects tends to be thicker than the defects in olivine. The SAED pattern of troilite shows that coincidence of the crystal directions among each troilite strip is much lower

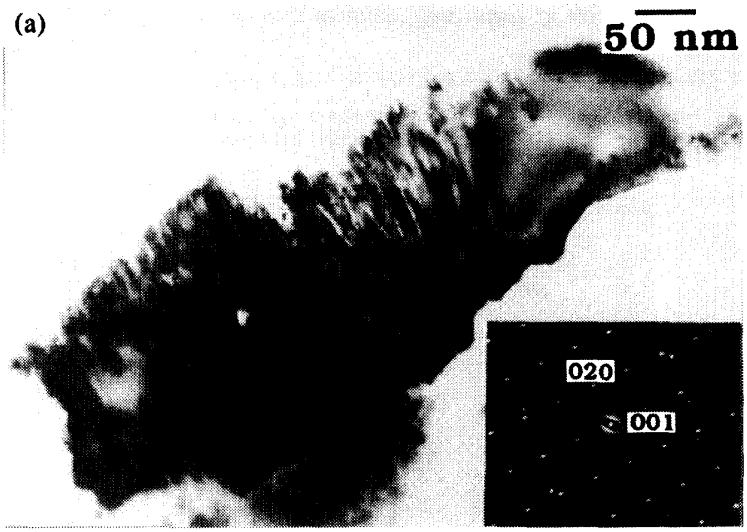

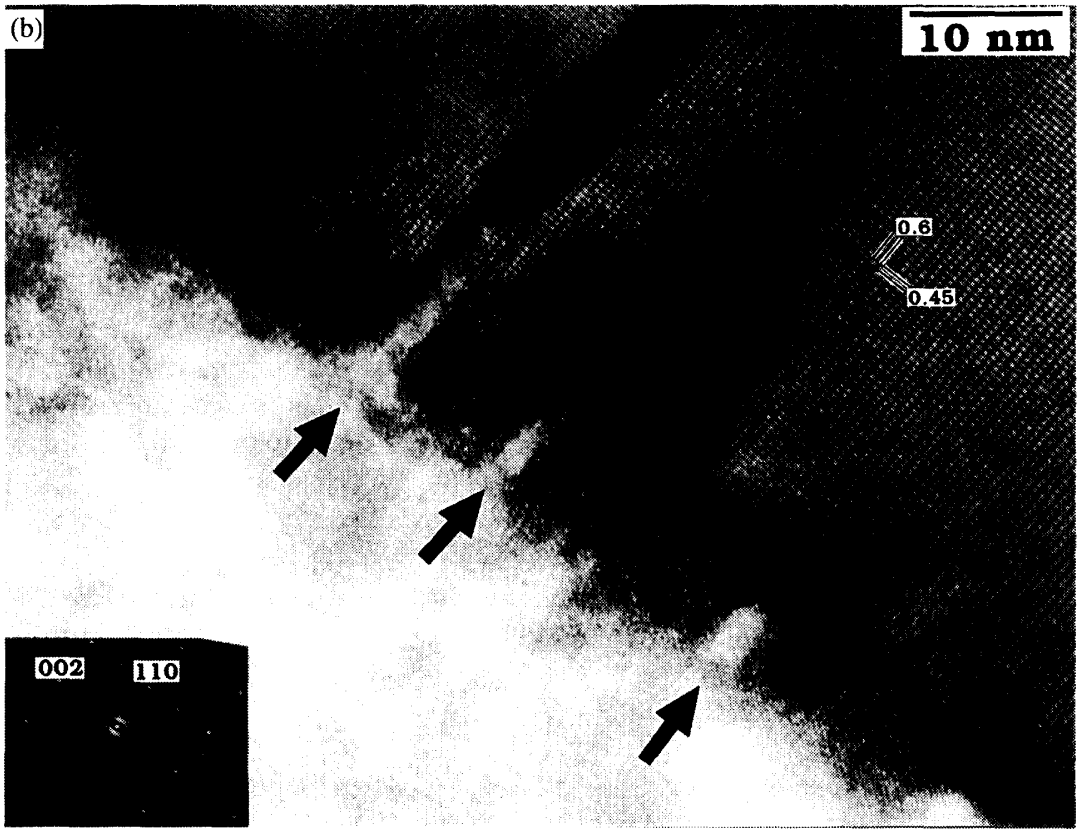

Fig. 7. (a) A bright-field TEM image of a matrix olivine crystal with abundant channel-like defects. Due to many defects, diffraction spots show streaks along c direction of olivine in the SAED pattern. (b) A high-resolution TEM image of a matrix olivine crystals with abundant channel-like defects. Nearly amorphous materials fill the channels. Pits on the surface of olivine indicate an incipient stage of formation of such defects. Units of the periodicities of lattice fringes are nm.*

than the case of olivine (Fig. 11b).

Poorly crystalline interstitial materials

There are abundant materials which fill the interstices of the above anhydrous minerals (Fig. 6). Because the interstitial materials show only a hallo pattern in SAED, they are named as poorly crystalline interstitial materials in this paper. The majority of the poorly crystalline interstitial materials are nearly amorphous under high

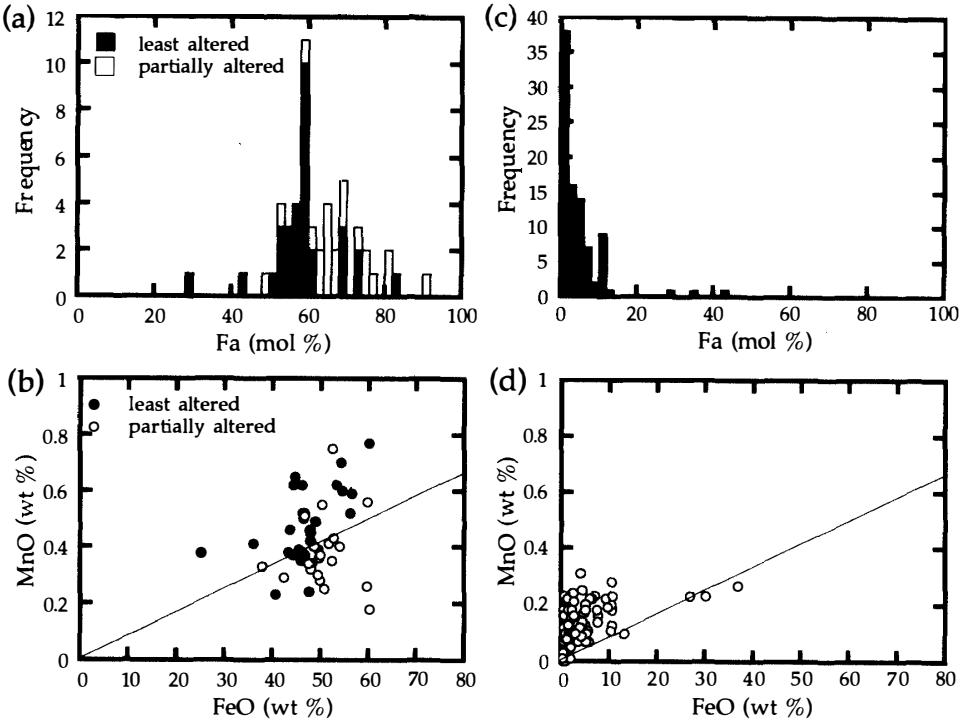

Fig. 8. Histograms of Fa mol% and an FeO vs MnO wt% diagrams of the matrix olivine (8a and 8b) and olivine in chondrules (8c and 8d). Data in 8a and 8b were measured by analytical electron microscope (AEM). In 8a and 8b, least altered: olivines without channel-like defects; partially altered: olivines with channel-like defects. (a) The majority of least altered olivines have Fa_{50}-Fa_{60}. Partially altered olivines are more Fa-rich. (b) Both kinds of olivine are plotted around the line with the ratio of solar Fe and Mn abundances. Data in 8c and 8d were measured by EPMA. (c) Most of olivine in chondrules is magnesian. (d) Most of olivine in chondrules is above the line with the ratio of solar Fe and Mn abundances.

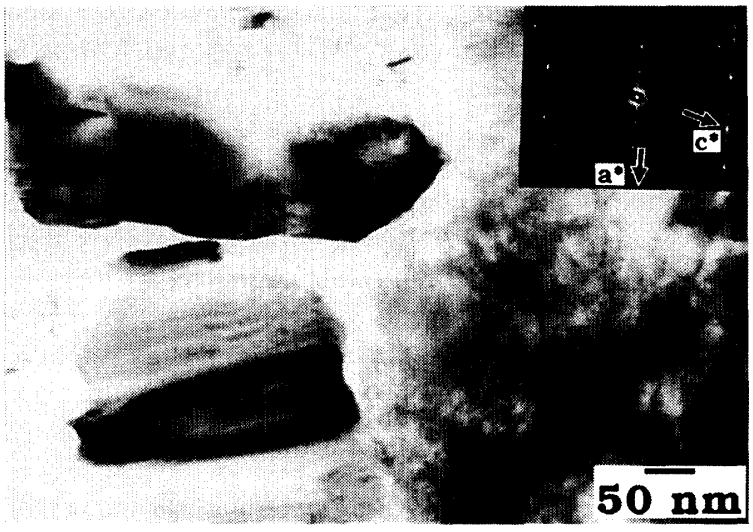

Fig. 9. A bright-field TEM image of matrix low-Ca pyroxene crystals. Inset shows a SAED pattern of upper low-Ca pyroxene crystal. The majority of low-Ca pyroxene is low-Ca clinopyroxene with a small amount of orthopyroxene lamellae.

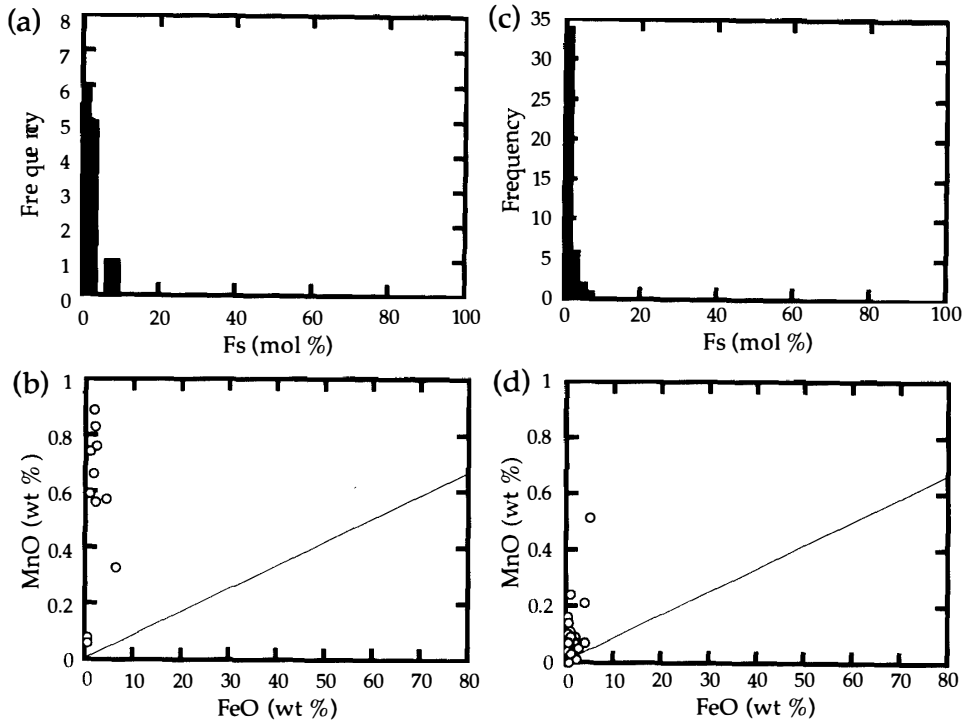

Fig. 10. Histograms of Fa mol % and an FeO vs MnO wt% diagrams of the matrix low-Ca pyroxene (a and b) and low-Ca pyroxene in chondrules (c and d). In a and b, data were measured by AEM. (a) The majority of low-Ca pyroxene is magnesian. (b) MnO contents of low-Ca pyroxene are relatively high, in stead of low FeO contents. Low-Ca pyroxene in matrix is above the line with the ratio of solar Fe and Mn abundances. In c and d, data were measured by EPMA. (c) The majority of low-Ca pyroxene is magnesian. (d) MnO contents of low-Ca pyroxene are lower than those of low-Ca pyroxene in matrix.

resolution. However, the interstitial materials which show fibrous appearances are sometimes observed (Figs. 6b and 12). Under high-resolution, typical fibrous materials are < 10 nm wide and < 50 nm long (Fig. 12). The fibrous materials sometimes develop in the peripheries of olivine, troilite, and Fe-rich amorphous patches (they may be altered Fe-Ni metal grains). Well-developed fibrous materials were observed in rare cases.

High-resolution TEM micrographs of the fibrous interstitial material indicate that there are ultrafine crystalline phases which have 0.7, and 1.0–1.2, (and rarely 1.4–1.5) nm diffuse lattice fringes. Most of the observed lattice fringes are 1.0–1.2 nm. Fibrous materials with 1.0–1.2 nm lattice fringes have thickness of 2–5 layers (Fig. 12b). Spacings vary within a single grain, and there are many defects and termination of layers in them. Occurrence of fibrous materials with 0.7 nm lattice fringes is similar to the materials with 1.0–1.2 nm lattice fringes. High-resolution TEM images also reveal that fine-grained materials with 0.4 nm lattice fringes are abundant within the interstitial materials. They seem to appear about 10 nm across equant grains (Fig. 12b). Their lattice fringes are faint but sharp, without change in their thickness. Because there are only lattice fringe data for these materials, it is impossible to identify mineral species for the materials. However, it is possible that the materials with 1.0–1.2 nm lattice fringes

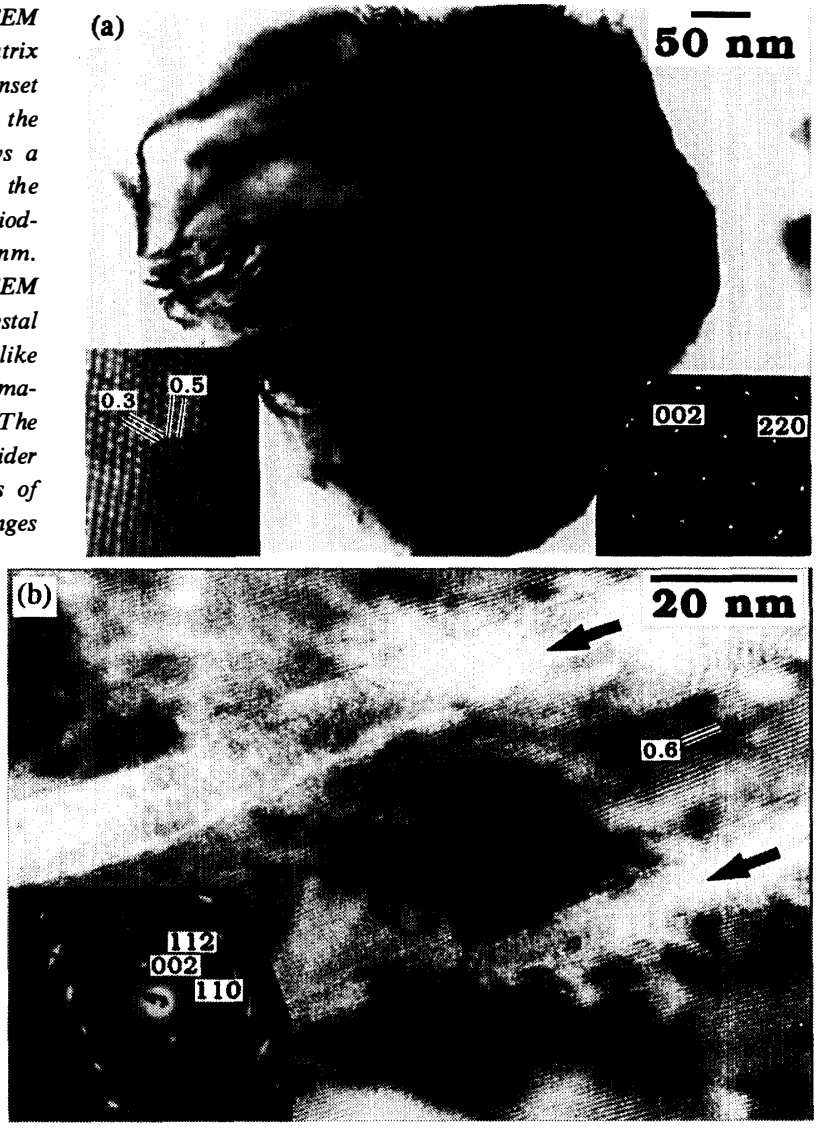

Fig. 11. (a) A bright-field TEM image of a subhedral matrix magnetite crystal. Right inset shows a SAED pattern of the crystal. The left inset shows a high-resolution image of the crystal. Units of the periodicities of lattice fringes are nm. (b) A high-resolution TEM image of a matrix FeS crystal with abundant channel-like defects. Nearly amorphous materials fill the channels. The widths of the channels are wider than those in olivine. Units of the periodicities of lattice fringes are nm.

may be smectite, and those with 0.4 nm goethite, those with 0.7 nm serpentine, and those with 1.4–1.5 chlorite. If this estimation is right, the poorly crystalline interstitial material is composed of abundant, almost amorphous Fe-rich material, with small amounts of saponite, goethite, and serpentine, with a trace amount of chlorite.

Each constituent phase of the poorly crystalline interstitial materials was too fine-grained to analyze, even using TEM with EDS system (analytical electron microscope: AEM). Electron beam diameter used for the interstitial materials was 0.15–0.3 μm. Therefore, AEM data can be interpreted as chemical composition of a mixture of phases as described above, like the case of microprobe analysis. FeO contents are positively correlated to SiO_2 content (Fig. 13a), as is the case of microprobe data (Fig. 3a). However, compositional ranges of both FeO and SiO_2 contents in AEM data are wider than those in microprobe data. There are many data with 60–80 wt% FeO and 10–20 wt% SiO_2. Only "limonite" veins and aggregates have such high FeO and low SiO_2 contents in microprobe data. These data suggest that the interstitial materials

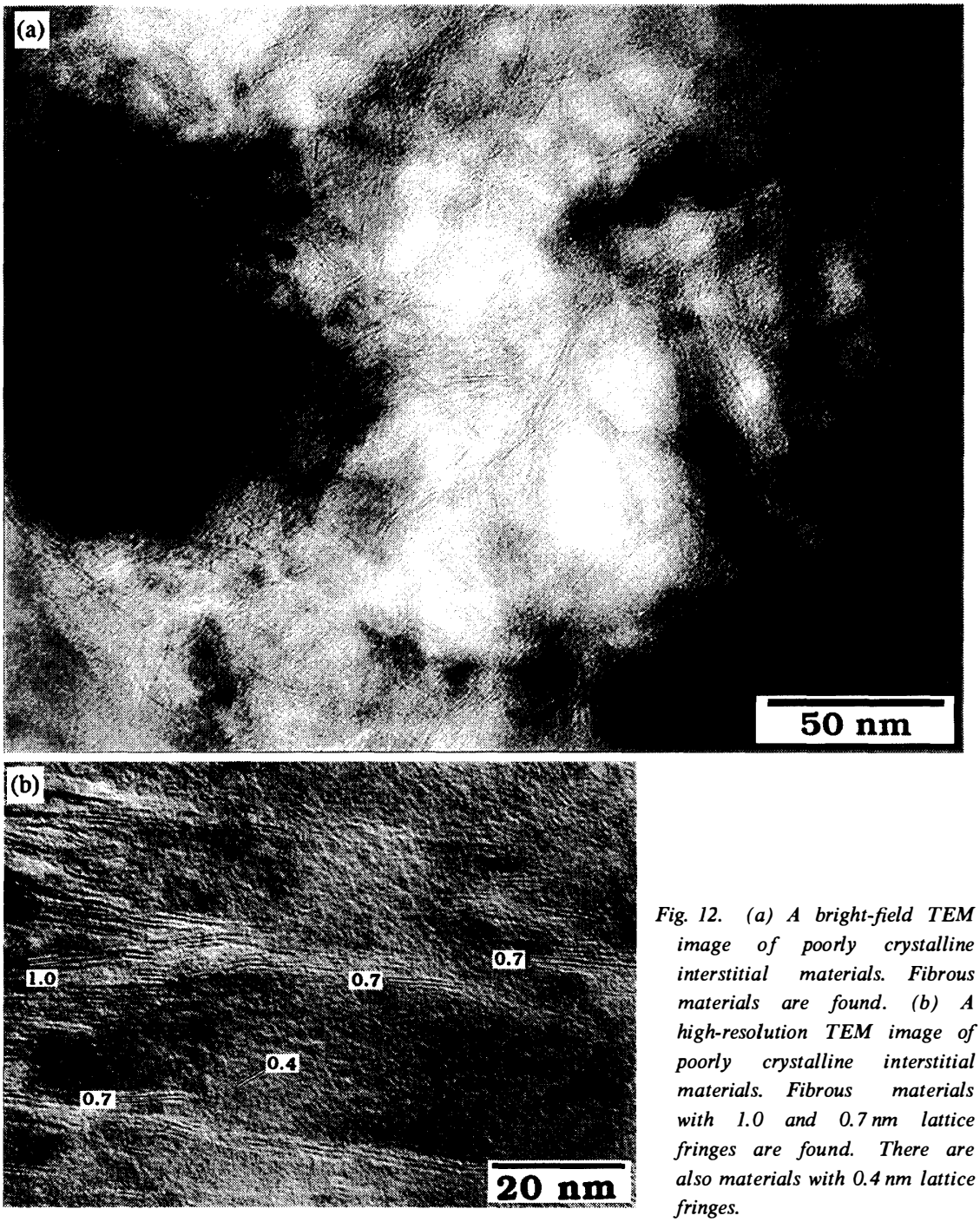

Fig. 12. (a) A bright-field TEM image of poorly crystalline interstitial materials. Fibrous materials are found. (b) A high-resolution TEM image of poorly crystalline interstitial materials. Fibrous materials with 1.0 and 0.7 nm lattice fringes are found. There are also materials with 0.4 nm lattice fringes.

contain the same materials which form the main constituent of "limonite" veins and aggregates (mainly Fe-rich hydroxides). There is also a counterpart of such high FeO and low SiO_2 contents (20–40 FeO and 40–50 SiO_2 wt%), that is also absent in microprobe data. The relation between Al_2O_3 and CaO contents and their compositional ranges are similar to those of microprobe data (Figs. 13b and 3b). There are analyses with higher Al_2O_3 contents in AEM data. These data are plotted on the

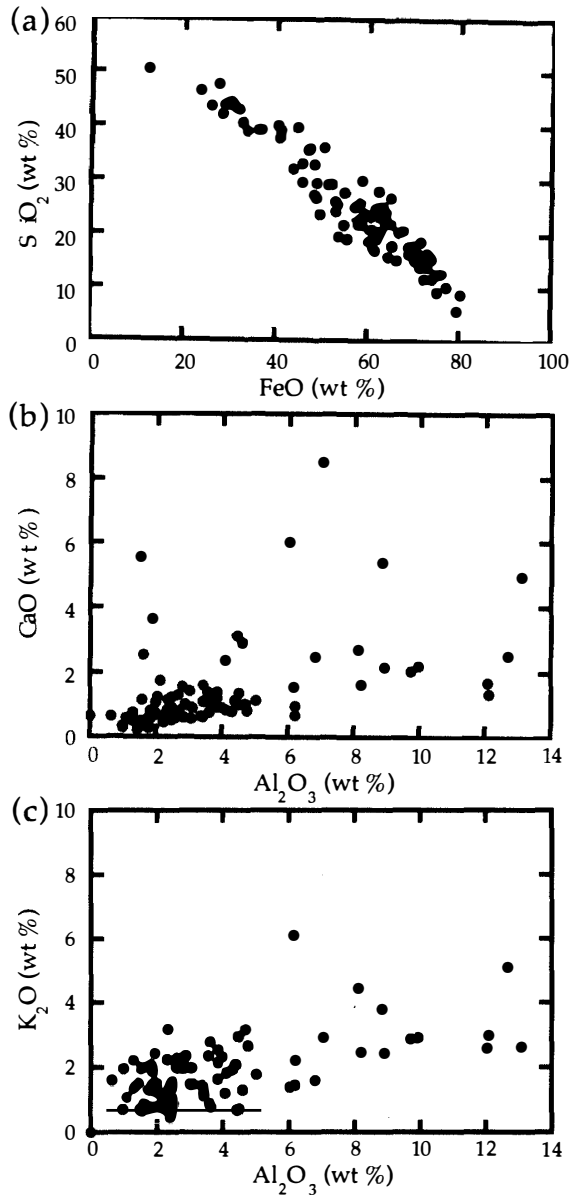

Fig. 13. The relations among some oxide wt% in the poorly crystalline interstitial materials. These data were measured by AEM.

extension of the trend shown in Fig. 3b. AEM data also support the idea that Al, Ca, and K are kept in the same carrier. On the other hand, analyses with low Al_2O_3 and high CaO contents are relatively rare. It is consistent that Ca-rich phase were rarely found during TEM observation. K_2O contents of the interstitial materials are much higher than those of microprobe data of fine-grained matrix (Figs. 13c and 3c). Fine-grained matrix is considered to be composed of K_2O enriched interstitial materials with K_2O free anhydrous minerals. Although Na was almost always below the detection limit in microprobe data, Na was rarely counted in AEM data (Table 2).

Major element compositions of sub-μm sized constituents in the fine-grained matrix are plotted on a ternary Si-Mg-Fe and [Mg+Fe]-Al-Si diagrams (Fig. 14). This figure reveals the reality of three hypothetical constituent components estimated from Fig. 5. Three major components are ferroan matrix olivine, poorly crystalline Fe-rich material,

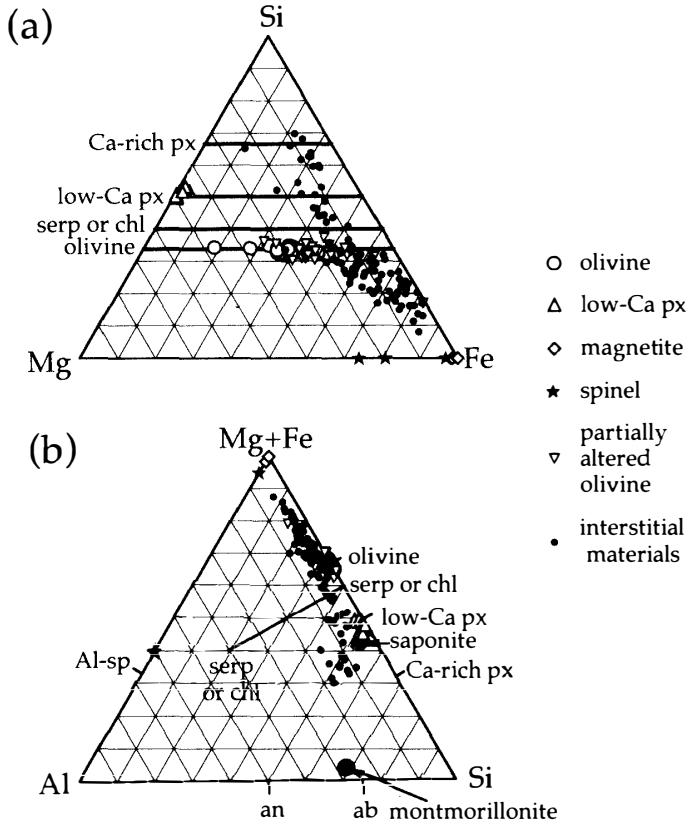

Fig. 14. Major element compositions of olivine, low-Ca pyroxene, magnetite, spinel group minerals, and poorly crystalline interstitial materials in the fine-grained matrix are plotted on a ternary Si-Mg-Fe and [Mg+Fe]-Al-Si diagrams. AEM data. Open circles: olivine with no channel-like defects; open triangles: low-Ca pyroxene; open diamonds: magnetite; filled stars: spinel group minerals (both chromian and aluminous spinels); open reverse triangles: olivine with channel-like defects; dots: poorly crystalline interstitial materials.

and Si-rich material which is also poorly crystalline but seems to contain more materials with smectite-like structure. As shown in Fig. 14b, montmorillonite-like materials may be included in the smectite-like structure, as well as saponite.

4. Discussion

4.1. Relict primary feature of the Colony matrix

As described in the previous sections, Colony is a heavily weathered meteorite, and in particular its matrix was modified by terrestrial weathering. However, there are some primary features which have been unaltered by terrestrial weathering. Chemical compositions of fine-grained matrix olivine give an estimation of primary compositional range of the matrix olivine in Colony. The majority of the matrix olivine crystals without planar defects have Fa_{50} to Fa_{60}, and olivine crystals with the defects tend to be more ferroan (Fig. 8). Magnesian fine-grained matrix olivine is rare. Because ferroan olivine is more susceptible to terrestrial weathering than magnesian olivine, magnesian olivines could survive if the Colony matrix primarily had contained abundant magnesian olivine. Therefore, magnesian matrix olivine was probably rare before suffering terrestrial weathering. It is difficult to estimate primary chemical compositions of the matrix olivine with planar defects, because poorly crystalline materials which fill the defects may have higher FeO contents (like "limonite") than host olivine

crystals (Fig. 8).

The matrices of ALHA77307 (CO3.1) and Lancé (CO3.4) were investigated using TEM by BREARLEY (1993) and KELLER and BUSECK (1990). There are four different types of the matrix olivine in ALHA77307. Fa mol% of the olivine is quite various (Fa_0-Fa_{70}). In Lancé, the matrix olivine has Fa_{40}-Fa_{60}. Considering only chemical compositions of matrix olivine, matrix olivine in Colony is similar to that in Lancé, rather than ALHA77307.

In the matrix of ALHA77307, the majority of matrix pyroxene are low-Ca pyroxene (En_{99}-En_{66}) (BREARLEY, 1993). Two of the three types of low-Ca pyroxene are orthopyroxene, and only one type is low-Ca clinopyroxene. Low-Ca pyroxene is not reported in KELLER and BUSECK (1990). In Colony, the majority of matrix pyroxene is low-Ca clinopyroxene with $En_{99\text{-}90}$ (Fig. 10). In these pyroxene, MnO contents are relatively high (0.6–0.9 wt%). Their crystal structure and chemical compositions are similar to LIME (low-Fe and Mn-enriched) pyroxenes (KLÖCK *et al.*, 1989; BREARLEY, 1993), although MnO contents are lower than those of typical LIME pyroxenes. It is not clear whether the absence of more ferroan low-Ca pyroxene in the matrix is a primary feature or not, because ferroan low-Ca pyroxene might be altered to poorly crystalline interstitial materials more rapidly than ferroan matrix olivine.

It is interesting to note that fine-grained, isolated, subhedral magnetite grains are present in the matrix, because μm-sized magnetite has not been found (RUBIN *et al.*, 1985). GOLDEN *et al.* (1995) found that magnetite can be formed by terrestrial weathering of Hoba nickel-iron meteorite. However, in the case of Colony, fine-grained matrix magnetite is probably primary, because only chromium except iron was detected by AEM and because nickel is preserved in magnetite if it was formed by terrestrial weathering (GOLDEN *et al.*, 1995).

Iron-nickel metal grains cannot be found in the matrix of Colony by TEM observation. It is also difficult to find μm-sized Fe-Ni metal by SEM and EPMA. Iron-nickel metal was probably altered to poorly crystalline interstitial materials, because it is very susceptible to terrestial weathering. Troilite can be identified by TEM although it suffers weathering. It is quite uncertain whether the matrix of Colony contains phyllosilicate before suffering weathering. Consequently, primary minerals which survive terrestrial weathering are: abundant olivine, less abundant low-Ca pyroxene, magnetite, with minor spinel group minerals (both chromian and aluminous spinels) and troilite, and rarer Ca-rich pyroxene. Microstructure and texture of these minerals, and their assemblages, are different from those in ALHA77307 and Lancé. However, these features in Colony are common to those in ALHA77307 than those in Lancé, although compositional range of matrix olivine in Colony is similar to that in Lancé.

4.2. Effects of terrestrial weathering on the Colony matrix

Alteration of Fe-Ni metal and its influence to the mineralogy of matrix

Under an optical microscope, fine-grained matrix of Colony is reddish brown to yellowish brown. This observation suggests that most of iron exists as Fe^{3+} in poorly crystalline interstitial materials. Because many Fe-Ni metal grains (and to a certain extent, FeS grains) in chondrules and matrix are altered by terrestrial weathering, Fe^{3+}-

(and Ni^{2+}-) bearing fluid was probably formed by the reactions between meteoric water and such Fe-Ni metal (and FeS) grains. Such Fe^{3+}-bearing fluid probably percolated into the fine-grained matrix directly around metal grains or through feeder veins (finally filled by "limonite") and the fluid probably reacted with anhydrous materials (mainly matrix olivine) to form the poorly crystalline interstitial materials. Supply of iron and sulfur from feeder veins is definite (Fig. 2 and Table 2). Silicon, magnesium, aluminum, nickel, calcium, and potassium seem to have leached through the veins (Fig. 2 and Table 2). Nickel and phosphorus also seem to have leached towards the veins but they seem to have precipitated in the veins (Table 2).

TEM observation suggests that the poorly crystalline interstitial materials are composed of Fe-enriched nearly amorphous material, minute phyllosilicates (mainly saponite, serpentine, chlorite, and rarer montomorillonite), and goethite (Fig. 12b). Presence of these phyllosilicates is probably the result of interaction between Fe-rich fluid and anhydrous minerals in the matrix. Goethite was probably formed during crystallization of the Fe-enriched nearly amorphous materials. It is not clear whether the Fe-enriched nearly amorphous materials contain minute ferrihydrite grains or not, although EPMA data suggest that Fe-hydroxide is the main constituent.

Microstructures of matrix olivine

Matrix olivine of Lancé contains channel-like defects which are parallel to [100] and [001] directions, and there are also planar defects parallel to the (100) plane (KELLER and BUSECK, 1990). Planar defects observed in the matrix olivine of Colony are always parallel to (001). Such planar defects parallel to (001) were reported in the lamellar iddingsite in terrestrial basalt (SMITH *et al.*, 1987). Such planar fissures are observed in the initial stage of iddingsite formation by the oxidative weathering of Fe-bearing olivine (Fa_{20}). YANO and NOGUCHI (1998) found planar defects parallel to (001) of olivine in a dehydrated unmelted micrometeorite. Because such olivine grains in the micrometeorite were formed by dehydration of phyllosilicates during atmospheric entry, the planar defects were formed after the micrometeorite was buried in snow. These defects quite resemble the planar defects found in the matrix olivine in Colony. Therefore, the defects found in this study probably indicate initial stage of iddingsite formation by terrestrial weathering.

Planar defects in olivine in CV chondrites have been reported (Mokoia: TOMEOKA and BUSECK, 1990; Grosnaja: KELLER and MCKAY, 1993; Bali: KELLER *et al.*, 1994; Vigarano: LEE *et al.*, 1996). All of these defects are parallel to the (100) plane, although the structures of each defect are different (stacking faults: Bali and Vigarano; smectite or Fe-oxide: Mokoia and Grosnaja). Matrix olivine only in Lancé contains defects which are not parallel to (100) as well as parallel ones. Based on the hydrothermal experiments, IISHI *et al.* (1997) estimated that defects parallel to (100) are formed under high pH conditions. If their estimation is true, it is reasonable that planar defects in the matrix olivine in Colony are parallel to (001) because the matrix olivine was weathered under approximately neutral to acidic conditions (alteration by meteoric water).

5. Conclusions

Colony is a badly weathered CO chondrite. Chemical composition (EPMA data) of the matrix of Colony changed by terrestrial weathering. EPMA data of matrix bulk composition suggest that the matrix is a mixture of an Fe-rich component, a component with olivine-like composition, and an Fe-poor, Si-rich component. TEM observation reveals that its matrix preserves some primary minerals. They are ferroan olivine, magnesian low-Ca pyroxene, magnetite, spinel group minerals (chromian and aluminous spinels), troilite, and rare Ca-rich pyroxene. Unaltered matrix olivine has Fa_{50}-Fa_{60}. Fe-rich component estimated from EPMA data is composed of abundant Fe-enriched nearly amorphous material, minute phyllosilicates (mainly saponite, serpentine, chlorite, and montomorillonite), and goethite. The Fe-poor, Si-rich component is also composed of basically the same materials in the Fe-rich component, but contains more phyllosilicates than Fe-rich one. Matrix olivine crystals often show planar defects which are almost parallel to (001). Such planar defects indicate that the initial iddingsitization of matrix olivine was by terrestrial weathering.

Acknowledgments

Scanning electron microscopy was performed at the Geological Institute, University of Tokyo. H. NAGAHARA, H. YOSHIDA and H. WADA are appreciated for their support to use the SEM. Lang's Fossils and Meteorites kindly sold a specimen of the Colony meteorite to one of the authors (TN). We thank A.E. RUBIN and an anonymous reviewer for their constructive comments for our manuscript. A.J. MARTIN is appreciated for his reading our manuscript. This work was supported by the Grant-in-Aid for Scientific Research, from the Ministry of Education, Science, Sports, and Culture, Japan (No. 06740408).

References

BENCE, A.E. and ALBEE, A.L. (1968): Empirical correction factors for the electron microanalysis of silicates and oxides. J. Geol., **76**, 382–403.

BREARLEY, A.J. (1993): Matrix and fine-grained rims in the unequilibrated CO3 chondrite ALHA77307: Origins and evidence for diverse, primitive nebular dust components. Geochim. Cosmochim. Acta, **57**, 1521–1550.

GOLDEN, D.C., MING, D.W. and ZOLENSKY, M.E. (1995): Chemistry and mineralogy of oxidation products on the surface of the Hoba nikel-iron meteorite. Meteoritics, **30**, 418–422.

IISHI, K., TORIGOE, K. and HAN, X. (1997): Oriented precipitate complexes in iron-rich olivines produced experimentally in aqueous oxidizing environment. Phys. Chem. Mineral., **25**, 8–14.

KELLER, L.P. and BUSECK, P.R. (1990): Matrix mineralogy of the Lancé CO3 carbonaceous chondrite: A transmission electron microscope study. Geochim. Cosmochim. Acta, **54**, 1155–1163.

KELLER, L.P. and MCKAY, D.S. (1993): Aqueous alteration of the Grosnaja CV3 carbonaceous chondrite. Meteoritics, **28**, 378.

KELLER, L.P., THOMAS, K.L., CLAYTON, R.N., MAYEDA, T.K., DEHART, J.M., and MCKAY, D.S. (1994): Aqueous alteration of the Bali CV3 chondrite: Evidence from mineralogy, mineral chemistry, and oxygen isotopic compositions. Geochim. Cosmochim. Acta, **58**, 5589–5598.

KLÖCK, W., THOMAS, K.L., MCKAY, D.S. and PALME, H. (1989): Unusual olivine and pyroxene composition

in interplanetary dust and unequilibrated ordinary chondrites. Nature, **339**, 126–128.

LEE, M.R., HUTCHISON, R. and GRAHAM, A.L. (1996): Aqueous alteration in the matrix of the Vigarano (CV 3) carbonaceous chondrite. Meteorit. Planet. Sci., **31**, 477–483.

LLOYD, G.E. (1987): Atomic number and crystallographic contrast with the SEM: A review of backscattered electron techniques. Mineral. Mag., **51**, 3–19.

NOGUCHI, T. (1995): Petrology and mineralogy of the PCA 91082 chondrite and its comparison with the Yamato-793495 (CR) chondrite. Proc. NIPR Symp. Antarct. Meteorites, **8**, 33–62.

RUBIN, A.E., JAMES, J.A., KECK, B.D., WEEKS, K.S., SEARS, D.W.G. and JAROSEWICH, E. (1985): The Colony meteorite and variations in CO3 chondrite properties. Meteoritics, **20**, 175–196.

SMITH, K.L., MILNES, A.R. and EGGLETON, R.A. (1987): Weathering of basalt: Formation of iddingsite. Clays Clay Mineral., **35**, 418–428.

SCOTT, E.R.D. and JONES, R.H. (1990): Disentangling nebular and asteroidal features of CO3 carbonaceous chondrites. Geochim. Cosmochim. Acta, **54**, 2485–2502.

SEARS, D.W.G., BATCHELOR, J.D., LU, J. and KECK, B.D. (1991): Metamorphism of CO and CO-like chondrites and comparisons with type 3 ordinary chondrites. Proc. NIPR Symp. Antarct. Meteorites, **4**, 319–343.

TOMEOKA, K. and BUSECK, P.R. (1990): Phyllosilicates in the Mokoia CV carbonaceous chondrite: Evidence for aqueous alteration in an oxidizing environment. Geochim. Cosmochim. Acta, **54**, 1745–1754.

YANO, H. and NOGUCHI, T. (1998): Sample processing and initial analysis techniques for Antarctic micrometeorites. Antarct. Meteorite Res., **11**, 136–154.

(Received November 4, 1998; Revised manuscript accepted December 17, 1998)